RESEARCH ARTICLE

Check for updates

In situ luminescence analysis: a new light on monitoring calcium phosphate phase transitions†‡

H. Terraschke, [iD] *[a] M. Rothe,[a] A.-M. Tsirigoni,[a] P. Lindenberg,[a] L. Ruiz Arana,[a] N. Heidenreich,[a,b] F. Bertram[b] and M. Etter[b]

In this work, *in situ* luminescence analysis was applied for the first time for monitoring the phase transitions of calcium phosphate (CaP) and confirmed by synchrotron *in situ* X-ray diffraction in addition to *in situ* infrared spectroscopy, with simultaneous measurements of pH and ion conductivity. Applying doped Ce^{3+} and Eu^{3+} as local coordination sensors, the high sensitivity of their emission spectra upon the changes in the coordination sphere of the doped cation sites enabled to detect the formation of amorphous calcium phosphate (ACP) and $Ca_5(PO_4)_3OH$, besides their subsequent transitions to $CaHPO_4 \cdot 2H_2O$ and $Ca_8H_2(PO_4)_6 \cdot 5H_2O$ under real reaction conditions. Calcium phosphates are widely present in mammals and understanding their phase transitions is important to comprehend the conversion between healthy and diseased tissues. *In situ* luminescence measurements are advantageous for allowing monitoring these phase transitions in a fast and sensitive fashion also in conventional laboratories, independent of synchrotron radiation.

1. Introduction

Efficiently monitoring the events occurring during the formation of solids in solutions including nucleation, crystal growth and formation of reaction intermediates as well as consequent phase transitions culminating in the crystallization of the final product require the application of *in situ* characterization techniques under real reaction conditions.[1–10] Studying the mechanism of chemical reactions by removing samples from the reactor during the synthesis process and analysing them *ex situ* is rather disadvantageous for offering only snapshots of the process with very limited time resolution, besides probably influencing the sample while preparing them for the *ex situ* analysis.[1,2] The formation and phase transitions of calcium phosphate (CaP) systems offer a critical example for

the importance of applying *in situ* techniques. Calcium phosphate derivatives are one of the main inorganic components in mammals and are widely used for producing medical implants and prosthesis.[11,12] For instance, amorphous calcium phosphate (ACP) is found in pathological tissues like heart valve calcifications,[11] $CaHPO_4 \cdot 2H_2O$ is proposed as an intermediate in bone mineralization,[11] $Ca_8H_2(PO_4)_6 \cdot 5H_2O$ is present in human dental and urinary calculi,[13] $CaHPO_4$ is used in bone cements,[14] while $Ca_5(PO_4)_3OH$ is used for coating orthopaedic and dental implants.[15] Therefore, understanding the formation and transition of the CaP phases is important for comprehending the transitions between healthy and diseased tissue as well as for predicting and preventing the degradation of implants and prosthesis in our bodies. In addition, studying the formation of CaP is essential for understanding the formation of amorphous pre-nucleation clusters, which is still a challenge for the currently accepted nucleation theories.[16–18] Since the phase transitions of CaP are extremely sensitive to variations in the environmental conditions such as temperature, pH and concentration, they should be ideally studied only *in situ* under real reaction conditions, in order to not disturb the investigated processes.[12] Up to now, different powerful *in situ* techniques have been reported in the literature for monitoring the mineralization mechanisms of CaP systems, as recently summarized by Pan *et al.*[12] Some of these *in situ* techniques are *in situ* pH measurements,[19] UV/Vis absorption spectroscopy,[20] Raman,[21] turbidity,[22] quartz crystal microbalance (QCM),[23] X-ray diffraction (XRD)[24] and X-ray absorption spectroscopy (XAS).[25] However, many of these techniques provide

[a]*Institut für Anorganische Chemie, Christian-Albrechts-Universität zu Kiel, Max-Eyth-Str. 2, 24118 Kiel, Germany. E-mail: hterraschke@ac.uni-kiel.de*
[b]*DESY Photon Science, Notkestr. 85, 22607 Hamburg, Germany*

†These results have been partially reported as posters and oral presentations at the conferences "18. Vortragstagung Fachgruppe Festkörperchemie und Materialforschung", September 19th–21st 2016, Innsbruck, Austria (DOI: 10.1002/zaac.201605095); "2nd joint workshop of MATsynCELL and C3", November 16th–17th 2015, Hamburg, Germany; "Summer School on Time-resolved and *In situ* Studies of Materials: Basics and Applications", August 22nd–29th 2015, Sellin, Island of Rügen, Germany.
‡Electronic supplementary information (ESI) available: Detailed description of experimental setup, complementary *ex situ* XRD and SEM measurements as well as additional results of *in situ* excitation spectra, IR spectroscopy and synchrotron-based XRD experiments. See DOI: 10.1039/c7qi00172j

This journal is © the Partner Organisations 2017

Inorg. Chem. Front., 2017, **4**, 1157–1165 | **1157**

information about phenomena occurring in the solution and not in the solid material, offer reduced time resolution or depend on synchrotron radiation, limiting their availability. A promising technique for monitoring chemical reactions consists of the *in situ* luminescence analysis of coordination sensors (ILACS) approach.[26] Within this technique, lanthanide ions as Eu^{3+}, Ce^{3+} and Tb^{3+} [27–29] are incorporated into the investigated materials during synthesis as local coordination sensors. Due to the sensitivity of their spectroscopic properties assigned to 5d → 4f or 4f → 4f electronic transitions to the coordination environment,[30,31] changes in the coordination of the cation sites during nucleation, crystal growth and phase transitions can be detected by measuring *in situ* luminescence applying fast charge-coupled device (ccd)-based detectors under real reaction conditions.[26] The fine structure and intensities of the luminescence bands assigned to the 4f → 4f electronic transitions *e.g.* the $^5D_0 → ^7F_{0-6}$ in Eu^{3+} are often applied as a spectroscopic probe for the local environment of these ions, especially due to the slight influence of the crystal field splitting on the respective energy levels.[32] However, a very high resolution of the luminescence spectra of the 4f → 4f transitions is necessary for analyzing the splitting behavior of their energy levels in detail and acquiring comprehensive information, for example, about the point symmetry and coordination polyhedron,[33] requiring often cooling the samples to liquid helium or liquid nitrogen temperatures. The parity allowed and highly intensive 5d → 4f electronic transitions *e.g.* in Ce^{3+}, on the other hand, are largely influenced by the covalence of the ligands (nephelauxetic effect) and crystal field splitting around the emissive ions.[34] Therefore, the luminescence bands assigned to the 5d → 4f transitions can vary from the UV to the red spectral range, depending on the host lattice and are able to reflect slight changes in the coordination environment around the emissive ions,[35] being ideally applied as a coordination sensor. Due to the above-mentioned reasons, the ILACS method is able to characterize not only ions in solution and amorphous or crystalline materials with high sensitivity and time resolution, but can be also flexibly applied at conventional laboratories or synchrotron facilities, for complementing other characterization techniques.[26]

In this work, the ILACS approach utilizes the 5d → 4f transitions of Ce^{3+} and the 4f → 4f transitions of Eu^{3+} for monitoring the formation of ACP and $Ca_5(PO_4)_3OH$ as well as their conversion to $CaHPO_4 \cdot 2H_2O$ and $Ca_8H_2(PO_4)_6 \cdot 5H_2O$. These processes have been confirmed here by *ex situ* and synchrotron-based *in situ* XRD, besides *in situ* measurements of pH value, ion conductivity and infrared (IR) spectroscopy. To the best of our knowledge, the application of *in situ* luminescence and IR techniques for monitoring CaP phase transitions as well as the optical properties of Ce^{3+} and Eu^{3+}-doped $CaHPO_4 \cdot 2H_2O$ and $Ca_8H_2(PO_4)_6 \cdot 5H_2O$ are reported here for the first time.

2. Experimental

For the synthesis of the different calcium phosphate phases, $Ca(NO_3)_2 \cdot 4H_2O$ (98.5+%, Merck KGaA, Darmstadt, Germany), $Eu(NO_3)_3 \cdot 6H_2O$ (99.9%, ChemPur Feinchemikalien und Forschungsbedarf GmbH, Karlsruhe, Germany), $Ce(NO_3)_3 \cdot 6H_2O$ (99.99%, Alfa Aesar GmbH & Co KG, Karlsruhe, Germany) and anhydrous $(NH_4)_2HPO_4$ (99+%, Merck KGaA, Darmstadt, Germany) have been used without further purification. The synthesis methods reported in this work consist of simplified co-precipitation techniques and the solutions have been freshly prepared for every trial, in which the $(Ca,Ln):PO_4^{3-}$ ratio was approximately 3:2. The concentrations and temperatures used specifically for each experiment are listed in Table 1. A detailed explanation of the assemblies used on experiments at the University of Kiel and at the Deutsches Elektronen-Synchrotron (DESY, Hamburg, Germany), respectively Setup A and Setup B, is supplied in the ESI.‡

2.1. Synthesis procedure with Setup A

In a typical synthesis procedure applying Setup A (experiments 1–8, Table 1), 20 mL of an aqueous solution of diammonium hydrogen phosphate are placed inside the reactor. Subsequently, 5–10 mL of an aqueous solution of calcium and cerium or europium nitrates were added to the reactor during the first 10 minutes of the reaction. During the dosing process, the temperature was kept at 10 °C and increased after

Table 1 Different experimental conditions applied for *in situ* monitoring the formation of calcium phosphate at the University of Kiel (Setup A), applying Ce^{3+} (experiments 1–5) and Eu^{3+} (experiments 6–8) as coordination sensors as well as experimental conditions applied for performing *in situ* XRD measurements at DESY (Setup B, experiments 9–10)

Experiment number	1	2	3	4	5	6	7	8	9	10
Added $Ca(NO_3)_2 \cdot 4H_2O$/mmol	1.06	1.06	1.06	1.06	1.06	1.06	1.06	3.53	7.60	6.33
Added $Ln(NO_3)_3 \cdot 6H_2O$/mmol	0.00	0.03	0.03	0.05	0.08	0.05	0.05	0.19	0.40	0.48
Volume of Ca/Ln solution/ml	5	5	5	5	5	5	5	10	5	5
Ce^{3+} doping concentration	0%	3%	3%	5%	7%	—	—	—	—	7%
Eu^{3+} doping concentration	—	—	—	—	—	3%	5%	5%	5%	—
Added $(NH_4)_2HPO_4$/mmol	0.7	0.7	0.7	0.7	0.7	0.7	0.7	2.9	5.3	4.5
Volume of $(NH_4)_2HPO_4$ solution/ml	20	20	20	20	20	20	20	20	40	40
Temperature/°C	10–80	10–80	10–80	10–80	10–80	10–80	10–80	10–80	~30–90	~30–90
Excitation wavelength/nm	—	280	—	—	280	395	395	—	365	365
Emission wavelength/nm	—	—	365	—	—	—	—	—	—	—
Beamline	—	—	—	—	—	—	—	—	P08	P02.1
Energy of synchrotron X-ray beam/keV	—	—	—	—	—	—	—	—	25	60

1158 | *Inorg. Chem. Front.*, 2017, **4**, 1157–1165

This journal is © the Partner Organisations 2017

few minutes to 80 °C. The reaction was then monitored by *in situ* measurements of pH value, ion conductivity, photoluminescence and infrared spectroscopy (Fig. S1 and S2‡). Because 80 °C is the temperature limit for the use of the pH and conductivity sensors, it is the highest temperature employed with this setup.

2.2. Synthesis procedure with Setup B

Similar to Setup A, 5 mL of a solution of calcium and cerium or europium nitrate in water was added with a rate of 0.5 mL min^{-1} to the reactor containing 40 mL of an aqueous solution of diammonium hydrogen phosphate (experiments 9 and 10, Table 1). In this context, it is important to mention that since the DESY reactor holder does not comprise a cooling system, the initial temperature of the reactor content was 30–35 °C. This high temperature is most probably caused by additional heating effects of the synchrotron X-ray beams and external excitation source for the luminescence measurements. For the DESY experiments (Fig. S3 and S4‡), it was necessary to increase the volume of the $(NH_4)_2HPO_4$ solution to 40 mL, in order to reach the filling volume required for the *in situ* XRD analysis applying the adapted glass reactor (Fig. S3 and S4‡). Within these experiments, the concentration of the solutions was also increased for improving the signal-to-noise ratio of the *in situ* XRD patterns.

3. Results and discussion

3.1. Preliminary *ex situ* experiments

For obtaining preliminary information on the changes of the calcium phosphate phase transitions during synthesis, samples were removed from the reactor of Setup A at determined reaction times and analysed by *ex situ* X-ray diffraction. *Ex situ* XRD patterns show the initial formation of a mixture of amorphous calcium phosphate and $Ca_5(PO_4)_3OH$ phase, which increasingly crystallizes to $Ca_5(PO_4)_3OH$[11] (Scheme 1) with an advanced reaction time and transforms after 7–10 min to $CaHPO_4·2H_2O$, changing again to $Ca_8H_2(PO_4)_6·5H_2O$ for temperatures above 57 °C (Fig. S5 and S6a,‡ experiment 1, Table 1). This trend is maintained, doping the Ca^{2+} sites with Ce^{3+} as a coordination sensor for concentrations up to 3% (Fig. S6b,‡ experiment 2, Table 1). On increasing the doping concentration to 5% (Fig. S6c,‡ experiment 5, Table 1), the

transition between $Ca_5(PO_4)_3OH$ and $CaHPO_4·2H_2O$ is shifted to 10–15 min. Interestingly, on further increasing the doping concentration to 7% (Fig. S6d,‡ experiment 5, Table 1), an additional transition from $Ca_5(PO_4)_3OH$ to $CaHPO_4$ at 7–10 min is observed, before the next conversion from $CaHPO_4$ to $CaHPO_4·2H_2O$ at 10–15 min. For 5% and 7% Ce^{3+}, $Ca_8H_2(PO_4)_6·5H_2O$ was also formed after 50 min. In this context, it is important to mention that increasing the doping concentration to 7% Ce^{3+}, caused the enhancement of the amorphisation, increasing the reaction period in which the ACP phase is stable. A probable explanation for this fact is the increase of the disorder on the calcium phosphate host lattice due to the introduction of Ce^{3+} ions within the Ca^{2+} site, due to their differences in ionic radii and charge.[36] Moreover, additional experiments have been carried out, for testing the influence of changing the type of coordination sensors from Ce^{3+} (experiment 4, Table 1) to Eu^{3+} (experiment 7, Table 1) on the calcium phosphate phase transitions.

As shown in Fig. S7,‡ the same phases have been obtained for the same reaction time such as a mixture of ACP and $Ca_5(PO_4)_3OH$ for $t = 10$ min as well as $CaHPO_4·2H_2O$ for $t = 15$ min and $t = 30$ min, for doping concentrations of 5%, showing no significant differences in the powder X-ray diffraction patterns measured for both coordination sensors Ce^{3+} and Eu^{3+}. In contrast, the concentration of the reactant solution strongly influences the calcium phosphate phase transitions (Fig. S8 and S9,‡ experiment 8, Table 1). On increasing the total concentration of the reactant solutions, reflections assigned to $CaHPO_4$ are observed within the ACP and $Ca_5(PO_4)_3OH$ phases, before the conversion to $CaHPO_4·2H_2O$. On increasing the temperature of the $CaHPO_4·2H_2O$ solution, the product loses two water molecules and is converted to anhydrous $CaHPO_4$ (Scheme 1). Scanning electron microscopy (SEM) images (Fig. S10‡) show the development of elongated needle-formed crystals agglomerated in discrete bundles at reaction time $t = 1$ min, identified as an ACP and $Ca_5(PO_4)_3OH$ mixture by *ex situ* XRD (Fig. S8‡). At $t = 20$ min, isolated single needle-formed crystals with a diameter of *ca.* 600 nm are observed, together with laminated plates, corresponding to the *ex situ* identified $CaHPO_4·2H_2O$ phase. At $t = 60$ min ($CaHPO_4$), rod-shaped crystals are formed, and the needles are still observed. All the samples doped with Eu^{3+} show a homogeneous red luminescence (Fig. S11‡), indicating that the coordination sensor was incorporated for all reaction times and *ex situ* luminescence measurements of the $^5D_0 \rightarrow {}^7F_0$ Eu^{3+} transition at *ca.* 580 nm show the double of the width of this peak for $Ca_5(PO_4)_3OH$ (two Ca^{2+} sites) in comparison with this peak measured for $CaHPO_4·2H_2O$ (one Ca^{2+} site), most probably due to the different numbers on crystallographic doping sites for Eu^{3+} (Fig. S12‡).[31]

3.2. *In situ* luminescence experiments

Ex situ characterization methods are helpful for gaining insights into the reaction mechanism, however, they consist only of discrete snapshots and do not deliver continuous information about the processes occurring inside the reaction.
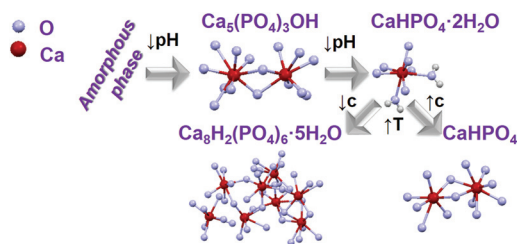
Scheme 1 Schematic representation of transition between different calcium phosphate phases by changing synthesis parameters as pH, temperature (T) and concentration (c).[11,16,37]

This journal is © the Partner Organisations 2017

Inorg. Chem. Front., 2017, **4**, 1157–1165 | **1159**

For instance, the *ex situ* XRD patterns presented here (Fig. S6–S8‡) show a time range where the phase transitions can occur, but not the exact time. In addition, the preparation procedure of the samples removed from the reactor for the *ex situ* characterization such as quenching, washing and drying might influence the product, generating possible divergences between the *ex situ* results and the actual phenomena occurring during the reactions.[2] For this reason, *in situ* luminescence measurements applying 3% of doping concentration have been carried out for the coordination sensors Ce^{3+} and Eu^{3+} (experiments 2 and 6, Table 1) and confirmed by different *in situ* analysis techniques. The doping concentration of 3% was chosen here due to the non-influence on the calcium phosphate phase transitions in comparison with undoped samples, demonstrated by preliminary *ex situ* XRD analysis (Fig. S6‡).

In general, as for the experiments applying Ce^{3+} as a coordination sensor (Fig. 1), no luminescence is initially detected upon the presence of pure $(NH_4)_2HPO_4$ solution in the reactor. On addition of the calcium and cerium solution, a broad emission band between *ca.* 310 nm and 440 nm with a maximum at 353 nm constantly rises during the first 10 minutes of the reaction, indicating the formation of the product (Fig. 1), identified as a mixture of ACP and $Ca_5(PO_4)OH$ by *ex situ* XRD analysis. This emission range is attributed in the literature to the Ce^{3+} electronic transition from the lowest 5d state to the ground state levels $^2F_{5/2}$ and $^2F_{7/2}$ in, for instance, calcium hydroxylapatite (HAp).[38] The non-symmetric shape of the Ce^{3+} band can be assigned to the simultaneous presence of secondary phases[39] *e.g.* ACP. After $t = 13$ min, the emission intensity starts to decrease and is slightly red shifted, corresponding to the transition to $CaHPO_4 \cdot 2H_2O$ indicated by *ex situ* XRD measurements (Fig. S6b‡).

The decrease of the emission intensity after $t = 13$ min could be justified by two different explanations. The first possible explanation is the increased quenching effect of the Ln^{3+} luminescence, caused by the two coordinating water molecules on the doped Ca^{2+} site on $CaHPO_4 \cdot 2H_2O$.[40,41] Within the second possible explanation, since the Ce^{3+} *in situ* emission spectra are recorded under a constant excitation at 280 nm, the decrease of the emission intensity could be caused by a shift of the excitation spectra during the conversion between different calcium phosphate phases. In order to verify this hypothesis, *in situ* excitation spectra ($\lambda_{em} = 365$ nm, experiment 3, Table 1) have been recorded under the same experimental conditions as Fig. 1 (Fig. S13–S15‡). As shown in Fig. S15,‡ the time-dependent profile of the *in situ* excitation spectra is very similar to the one of the *in situ* emission spectra and no significant shift in the excitation spectra is observed. Here, the decrease of the intensity of the excitation bands is singly related to the same intensity decrease of the respective emission band at 365 nm. Therefore, this hypothesis can be ruled out and the variation of the time-dependent emission intensity can be associated with the attachment and detachment of quenching water molecules within the coordination spheres of the lanthanide-based coordination sensors. The red shift of the Ce^{3+} emission band upon the formation of $CaHPO_4 \cdot 2H_2O$, could indicate that this compound presents a higher coordination number or a shorter average bond length with the coordinating oxygen ions than in the previously formed ACP phase, since it is not the case for $Ca_5(PO_4)_3(OH)$.[42] However, due to the lack of long-range order and Rontgen amorphous character of the ACP phase, very little structural information is available about this phase.[43,44] In this context, it is important to note that *ex situ* XRD analysis shows the formation of $CaHPO_4 \cdot 2H_2O$ after $t = 10$ min (Fig. S6B‡), while *in situ* measurements locate this phase transition at $t = 13$ min. As observed in our previous work,[45] the sample preparation conditions can lead to the *ex situ* conversion of the phase mixture to the stable $CaHPO_4 \cdot 2H_2O$ compound. Within the *in situ* luminescence measurements, the Ce^{3+} emission intensity remains approximately constant at $t = 20–40$ min, indicating no significant structural change in this time range, in agreement with the respective *ex situ* XRD patterns (Fig. S6b‡). After $t = 40$ min, the temperature starts to increase and the emission intensity starts to decrease, caused by thermal quenching effects and confirmed by the consecutive increase of the emission intensity after cooling the system down to room temperature (Fig. 1 and S5‡). At approximately, $t = 51$ min, the emission intensity slightly increases and decreases again, indicating additional structural changes in
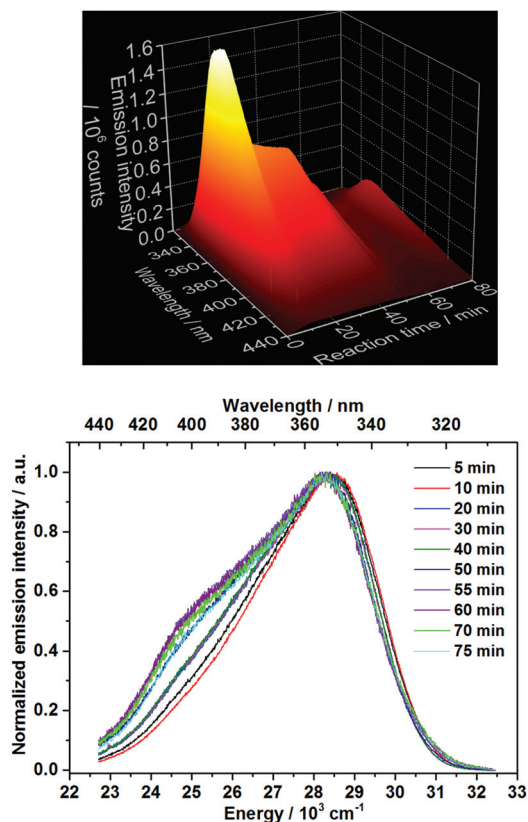

Fig. 1 Top: *In situ* emission spectrum recorded during calcium phosphate phase transitions applying 3% Ce^{3+} as a coordination sensor (λ_{ex} = 280 nm). Bottom: Normalized emission spectra for selected reaction times (experiment 2, Table 1).

1160 | *Inorg. Chem. Front.*, 2017, **4**, 1157–1165

This journal is © the Partner Organisations 2017

the cation environment and therefore a new phase transition by reaching the temperature of *ca.* 60 °C. This phase transition coincides with the results obtained by *ex situ* XRD analysis (Fig. S6b‡), showing the conversion from $CaHPO_4 \cdot 2H_2O$ to $Ca_8H_2(PO_4)_6 \cdot 5H_2O$ between t = 50 and 55 min. The temperature of approximately 60 °C also coincides with the decomposition temperature of $CaHPO_4 \cdot 2H_2O$ on the *in situ* XRD data measured at the DESY synchrotron facility, discussed in detail below. The formation of the new phase is also indicated by the rise of an additional Ce^{3+} emission band at 24 500 cm^{-1} (Fig. 1), which is not related to the increase of the temperature, since it is still observed after the system was cooled down to room temperature. The rise of additional Ce^{3+} emission bands is in agreement with the enhancement of crystallographic available Ca^{2+} doping sites for the coordination sensors, increasing from one Ca^{2+} site in $CaHPO_4 \cdot 2H_2O$ to eight Ca^{2+} sites on $Ca_8H_2(PO_4)_6 \cdot 5H_2O$.[41] The red shift of the Ce^{3+} emission bands can be explained by the decrease of the average bond lengths between the calcium and coordinating oxygen ions within $Ca_8H_2(PO_4)_6 \cdot 5H_2O$,[46] caused by the so-called nephelauxetic effect.[39] Moreover, additional structural information can explain the spectroscopic behavior, in which the increase of the emission intensity at t = 51 min during the phase transition occurs most probably due to the decrease of the number of the quenching water molecules on the coordination sphere of the coordination sensor during the conversion from $CaHPO_4 \cdot 2H_2O$ to $Ca_8H_2(PO_4)_6 \cdot 5H_2O$, further decreasing afterwards due to thermal quenching effects.

Fig. 2 shows the time-dependent emission spectra applying Eu^{3+} as coordination sensors. Since these measurements have been carried out in solution, a strong quenching effect is observed, caused by the non-radiative depopulation of the excited states of Eu^{3+} due to the vibrational energy transfer involving the high energy vibrations of the OH oscillator from the H_2O solvent molecules.[47] This quenching effect results in the low intensity of the Eu^{3+} emission and consequent

enhanced loss of resolution, differing therefore from previously reported emission spectra of Eu^{3+} doped ACP[48] and $Ca_5(PO_4)_3OH$.[49–51] Additional causes for deviations in comparison with luminescence spectra of Eu^{3+}-doped calcium phosphates reported in the literature are different synthesis methods applied and therefore different particle sizes, doping concentrations, measurement temperatures and excitation wavelengths. As mentioned above, no spectral data about the luminescence properties of Eu^{3+} doped $CaHPO_4 \cdot 2H_2O$ and $Ca_8H_2(PO_4)_6 \cdot 5H_2O$ is available in the literature so far for comparison. The intensity of the $^5D_0 \rightarrow {}^7F_J$ (J = 1–4) Eu^{3+} transitions shows the same behavior as for the Ce^{3+} experiments. Hence, the continuous increase of the intensity in the first 10 minutes (Fig. 3) indicates the formation of a solid material, assigned to a mixture of ACP and $Ca_5(PO_4)_3OH$ by *ex situ* XRD (Fig. S6b‡) followed by a decrease of intensity at $t \approx 13$ min, indicating the conversion to $CaHPO_4 \cdot 2H_2O$, most probably caused by the quenching effect of the two coordinating water molecules. Also for the Eu^{3+} coordination sensor, the intensity remains constant up to approximately t = 51 min, reaching the temperature of 60 °C, when an additional intensity oscillation indicates the additional phase transition to $Ca_8H_2(PO_4)_6 \cdot 5H_2O$.

Fig. 3 shows in addition the confirmation of the structural changes detected by *in situ* luminescence measurements discussed above by comparison with *in situ* pH value and ion conductivity measurements as well as *in situ* infrared spectroscopy. Up to t = 10 min, the conductivity increases during the addition of extra ions during the introduction of the solution containing calcium and cerium or europium nitrate. This solution addition also causes the decrease of the pH, due to the acidity of the nitrate solution. Initially, $Ca_5(PO_4)_3OH$ and ACP $(Ca_9(PO_4)_6)$[11,42] formed, according to the *ex situ* XRD measurements (Fig. S6b‡). The higher pH of the initial phosphate solution inside the reactor (pH = 5.85, Fig. 3, orange curve) can cause the deprotonation of the phosphate anions, stabilizing the PO_4^{3-} species and therefore, the $Ca_5(PO_4)_3OH$ and ACP phases.[11] Upon the addition of more acidic nitrate solution and consequent decrease of the pH value, the reflec-
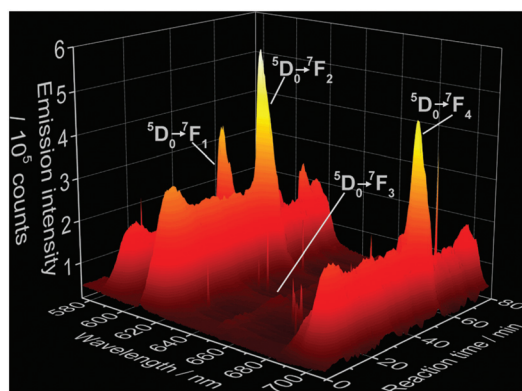

Fig. 2 Time-dependence of $^5D_0 \rightarrow {}^7F_J$ (J = 1–4) electronic transitions of Eu^{3+} during the formation of doped calcium phosphate (λ_{ex} = 395 nm, experiment 5, Table 1). Sharper peaks parallel to the Eu^{3+} emission bands are assigned to measurement artifacts originated by the CCD detector.
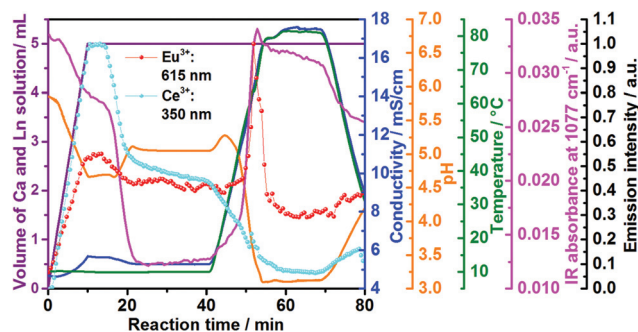

Fig. 3 Time dependence of the emission intensity of Ce^{3+} (light blue curve) and Eu^{3+} (red curve) doped calcium phosphate, *in situ* ion conductivity (dark blue curve), *in situ* pH (orange curve) and IR intensity at 1077 cm^{-1} (pink curve) in comparison with the volume of the Ca^{2+} and Ln^{3+} solution (violett curve) to the reactor containing aqueous $(NH_4)_2HPO_4$ (experiments 2 and 6, Table 1).
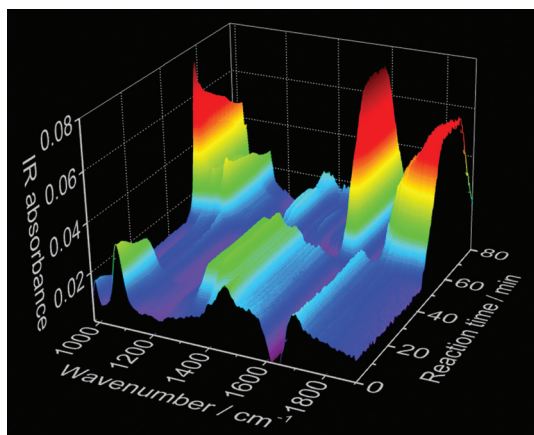
Fig. 4 Time-dependence of *in situ* IR spectroscopy measurements during the synthesis of Ce^{3+}-doped calcium phosphate (experiment 2, Table 1).

tions assigned to $Ca_5(PO_4)_3OH$ become more clear and with further decrease of the pH value, the phosphate ions are partially protonated,[11] resulting in the conversion from $Ca_5(PO_4)_3OH$ to $CaHPO_4 \cdot 2H_2O$. This conversion also causes a slight decrease in the conductivity due to the uptake of the H^+ ions for $CaHPO_4 \cdot 2H_2O$ formation. Similarly to *in situ* luminescence measurements, *in situ* pH and ion conductivity remain nearly constant between t = 20–40 min, indicating no significant structural changes and the stabilization of the $CaHPO_4 \cdot 2H_2O$ phase (Fig. S6b‡). After t = 40 min, the large oscillations on pH values and ion conductivity are strongly influenced by the temperature, masking additional structural changes. Also interesting are the changes in the IR absorption bands during the calcium phosphate phase transitions (Fig. 3 and 4), displayed in detail in the ESI (Fig. S16‡). Fig. 3, for instance, shows the time-dependence of the IR absorption band at 1077 cm^{-1}, assigned to the δPOH vibrations within the $(NH_4)_2HPO_4$ solution.[52] Initially, the intensity of this band decreases due to the uptake of phosphate ions from the solution to form ACP and $Ca_5(PO_4)_3OH$, after deprotonation. The decrease of this IR band is also caused by the uptake of HPO_4^{2-} ions for the formation of $CaHPO_4 \cdot 2H_2O$ and $Ca_8H_2(PO_4)_6 \cdot 5H_2O$ ($Ca_8(HPO_4)_2(PO_4)_4 \cdot 5H_2O$).

3.3. *In situ* X-ray diffraction and light transmission measurements

As mentioned above, since samples analyzed *ex situ* can be influenced by the preparation procedure, *in situ* XRD measurements at the P02.1[53] and P08[54] beamlines at DESY in Hamburg, Germany, have been additionally carried out (Fig. S17–S21‡). In general for all *in situ* experiments, an increase of the background at low 2θ angles is observed upon the addition of the solution containing calcium and europium or cerium nitrate to the $(NH_4)_2HPO_4$ solution. This background increase is assigned to the formation of an amorphous phase,[55] coinciding with the formation of the combined ACP and $Ca_5(PO_4)_3OH$ phases demonstrated by the *ex situ* XRD

measurements displayed in Fig. S6.‡ Most probably, the reflections assigned to $Ca_5(PO_4)_3OH$ have not been detected within the *in situ* XRD patterns, because (i) its degree of crystallinity is rather low, (ii) the crystallite size is too small or (iii) this phase is generated only during the *ex situ* preparation of the samples for the XRD measurements. Even though the broad reflections of the $Ca_5(PO_4)_3OH$ phase in Fig. S6‡ indicate the validation of hypotheses (i) and (ii), additional experiments are necessary to verify these theories. After the rise of the ACP background, this signal starts to decrease, while the reflections of $CaHPO_4 \cdot 2H_2O$ (Fig. S17‡) start to increase. At approximately 63 °C, $CaHPO_4 \cdot 2H_2O$ starts to decompose, simultaneously with the increase of the $Ca_8H_2(PO_4)_6 \cdot 5H_2O$ reflections (Fig. S17‡).

According to Engelke *et al.*,[5] different mechanisms can govern the transformation between different phases during the formation of solid materials in solution. These mechanisms are, for instance, (i) a direct solid–solid transition, (ii) the first phase completely dissolves before the emerging phase nucleates and crystallizes from the solution and (iii) the formation of the single phase consists of completely separated processes. Fig. S18‡ shows, for example, that the intensity of the ACP XRD signal is highly correlated with the intensity of the (0,2,0) reflection of the $CaHPO_4 \cdot 2H_2O$ phase. Hence, the onset of the decay of the ACP occurs simultaneously with the onset of the crystallization of the $CaHPO_4 \cdot 2H_2O$ phase, indicating that $CaHPO_4 \cdot 2H_2O$ grows and the intensity of these reflections increases at the cost of the ACP phase. Therefore, the hypothesis (iii) can be ruled out. If hypothesis (ii) were true, the ACP signal would partially or completely disappear before the onset of the $CaHPO_4 \cdot 2H_2O$ crystallization and the curves of the normalized reflection intensities of these two phases would not intersect. A similar behaviour can be observed comparing the correlation of the intensities of the reflections assigned to the $CaHPO_4 \cdot 2H_2O$ and $Ca_8H_2(PO_4)_6 \cdot 5H_2O$ phases. The normalized reflection intensities of the respective transitions show, however, intersections at 0.5 and 0.6 (Fig. S18‡), indicating that the respective conversions from ACP to $CaHPO_4 \cdot 2H_2O$ and from $CaHPO_4 \cdot 2H_2O$ to $Ca_8H_2(PO_4)_6 \cdot 5H_2O$ are rather governed by solid–solid phase transitions, in agreement with hypothesis (i).[56]

Fig. S18‡ shows the normalized intensity of XRD intensities (λ = 0.4959 Å) at 0.5732° 2θ (green curve), assigned to the amorphous phase,[55] 1.5142° 2θ (pink curve), assigned to the (1,0,0) reflection of $Ca_8H_2(PO_4)_6 \cdot 5H_2O$[46] (Fig. S17‡) and 3.7471° 2θ (violet curve), assigned to the (0,2,0) reflection of $CaHPO_4 \cdot 2H_2O$[41] (Fig. S19‡), measured *in situ* during the synthesis of Eu^{3+}-doped calcium phosphate at the DESY P08 beamline (experiment 9, Table 1). This diagram shows the initial formation of amorphous calcium phosphate, which converts at t = 7.5–13.5 min to $CaHPO_4 \cdot 2H_2O$, growing further up to t = 22 min. When the temperature is increased to 63 °C, the intensity of the reflection assigned to $CaHPO_4 \cdot 2H_2O$ starts to decrease, upon the increase of the reflection assigned to the $Ca_8H_2(PO_4)_6 \cdot 5H_2O$ phase. In this context, it is important to note that the increase of the intensity of the reflection at

1162 | *Inorg. Chem. Front.*, 2017, **4**, 1157–1165

This journal is © the Partner Organisations 2017

1.5142° 2θ (pink curve) at t = 0–14 min occurs due to the overlap with the broad signal of the amorphous phase and not because of a premature formation of $Ca_8H_2(PO_4)_6\cdot5H_2O$. As explained within section 2.2, slight shifts in the time range of the phase transitions in comparison with experiments carried out with Setup A might be assigned to the adaptation of the experimental conditions, necessary for performing these experiments at the synchrotron facility.

The formation of the amorphous phase at t = 1 min is also detected by the simultaneous increase of the intensity of the Eu^{3+} $^5D_0 \rightarrow {}^7F_2$ electronic transition at 613 nm. The changes in the intensity ratio between the $^5D_0 \rightarrow {}^7F_2$ and $^5D_0 \rightarrow {}^7F_1$ transitions indicate changes in the symmetry around the cation sites during the formation of the amorphous phase (Fig. S19‡).

Similar to Fig. S18,‡ Fig. 5 shows the initial formation of ACP during the synthesis of Ce^{3+}-doped calcium phosphate, which converts at t = 9–14.5 min to $CaHPO_4\cdot2H_2O$ (Fig. S21‡), growing further up to approximately t = 23 min. Similar to that indicated in Fig. S6,‡ a possible explanation for the longer stabilization of the amorphous phase on the measurements in Fig. 5 (7% Ln^{3+}) than the measurements in Fig. S18‡ (5% Ln^{3+}) could be the higher amount of coordination sensors. Because the differences in ionic radii and charge between Ln^{3+} and Ca^{2+} ions, doping trivalent lanthanides within calcium phosphate could increase the disorder within the solid material, delaying crystallization. When the temperature is increased to *ca.* 60 °C, the intensity of the reflection assigned to $CaHPO_4\cdot2H_2O$ decreases, upon the increase of the reflection assigned to the $Ca_8H_2(PO_4)_6\cdot5H_2O$ phase (Fig. S20‡). As previously mentioned in Fig. S18,‡ the increase of the intensity of the reflection at 0.6347° 2θ (pink curve) at t = 0–20 min occurs due to an overlap with the broad signal of the amorphous phase and not because of a premature formation of $Ca_8H_2(PO_4)_6\cdot5H_2O$ (Fig. S21‡). The intensity of the reflection

assigned to $Ca_8H_2(PO_4)_6\cdot5H_2O$ reaches its maximum at the maximum temperature of 100 °C and decreases afterward turning the heating system off at t = 28.5 min, which could be caused by (i) a decrease of crystallinity or (ii) the partial dissolution of the product. Hence, the simultaneously performed *in situ* measurements of light transmission through the reaction solution offer additional insights into this open question and is discussed in detail in Fig. 6. At t = 55 min, a 25% NH_3 solution was added to the reactor in order to evaluate the effect of the increase of the pH in this reaction stage. However, the addition of NH_3 has not shown a significant influence on the calcium phosphate phase transitions.

As explained in section 1.2 of the ESI,‡ for these experiments, a 365 nm light source was used for irradiating the reactor, while an optical fiber submersed in the reactor content and connected to a CCD detector, was applied for measuring the intensity of the light source transmitted through the solution during the reaction. Upon the addition of the calcium and cerium nitrate solution to the reactor containing $(NH_4)_2HPO_4$ (Fig. 6), the intensity of the light source firstly increases, probably due to a brief diluting effect caused by the addition of the second solution to the reactor. The formation of solid material at t = 0.5 min is detected by the strong decrease of the intensity of the light source, caused by the increase of the turbidity of the solution, blocking light transmission.[45] The light transmission decreases further up to $t \approx$ 14 min, during the formation of $CaHPO_4\cdot2H_2O$ (Fig. 5), and is rather constant while the growth of $CaHPO_4\cdot2H_2O$ stabilizes. At approximately t = 23 min, the light transmission starts to decrease again, coinciding with the formation of $Ca_8H_2(PO_4)_6\cdot5H_2O$ (Fig. 5). Even though the intensity of the reflections decreases during the cooling process, the further decrease of the light intensity indicates an increase in the turbidity of the solution, ruling out the hypothesis of product dissolution, discussed in Fig. 5. The oscillation of the intensity of the light source and signals of all other sensors at t = 28.5 min are assigned to the oscillation of the temperature by turning off the heating system.
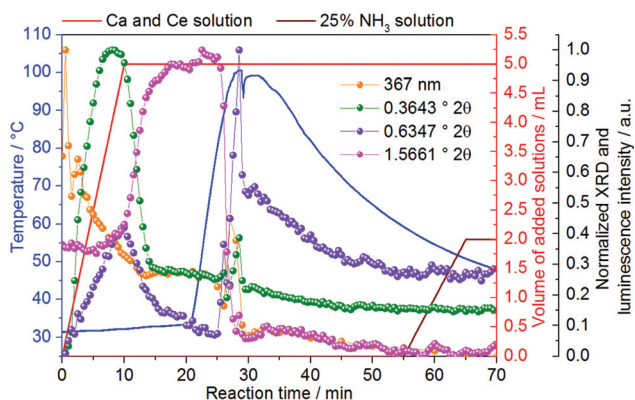

Fig. 5 Normalized intensity of XRD reflections (λ = 0.2075 Å) at 0.3643° 2θ (green curve), assigned to the amorphous phase,[55] 0.6347° 2θ (pink curve), assigned to the (1,0,0) reflection of $Ca_8H_2(PO_4)_6\cdot5H_2O$[46] (Fig. S20‡) and 1.5661° 2θ (violet curve), assigned to the (0,2,0) reflection of $CaHPO_4\cdot2H_2O$[41] (Fig. S20‡), measured *in situ* during the formation of Ce^{3+}-doped calcium phosphate at the DESY P02.1 beamline (experiment 10, Table 1).
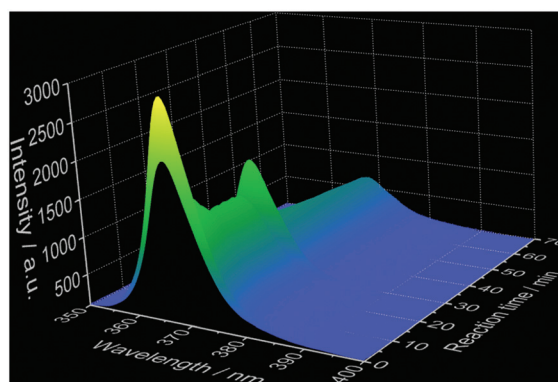

Fig. 6 Time-dependent light transmission of a 365 nm light source during the synthesis of Ce^{3+}-doped calcium phosphate (experiment 10, Table 1).

This journal is © the Partner Organisations 2017

Inorg. Chem. Front., 2017, **4**, 1157–1165 | **1163**

4. Conclusions

This work introduces the recently developed ILACS[26] *in situ* luminescence approach as a new technique for characterizing the phase transitions in calcium phosphate. Calcium phosphate is a major inorganic component of the human body,[11] often found in both healthy and pathologic tissues such as bones and teeth, heart calcifications or caries. Here, the ILACS approach explored the coordination sensitive emissive f–d and f–f electronic transitions on, respectively, Ce^{3+} and Eu^{3+} as local sensors for delivering information about structural changes around the doped cation sites. Therewith, it was possible to detect the formation of ACP and $Ca_5(PO_4)_3OH$ as well as their subsequent conversion to $CaHPO_4 \cdot 2H_2O$ and $Ca_8H_2(PO_4)_6 \cdot 5H_2O$. The detection of these phase transitions has been confirmed by additional characterization methods as *in situ* measurements of pH value, ion conductivity, IR spectroscopy, besides *ex situ* and synchrotron-based *in situ* techniques. Upon addition of the solutions of calcium and europium or cerium nitrates to $(NH_4)_2HPO_4$, a mixture of ACP and $Ca_5(PO_4)_3OH$ is formed, converted to $CaHPO_4 \cdot 2H_2O$, most probably due to a decrease of the pH. On increasing the temperature, $CaHPO_4 \cdot 2H_2O$ is decomposed upon the formation of $CaHPO_4$ with a higher reactant concentration and $Ca_8H_2(PO_4)_6 \cdot 5H_2O$ with a lower reactant concentration. Understanding the phase transitions of calcium phosphate is important for, for instance, comprehending and treating diseases.

Acknowledgements

References

1 N. Pienack and W. Bensch, *Angew. Chem., Int. Ed.*, 2011, **50**, 2014 and references therein.

2 H. Terraschke, M. Rothe and P. Lindenberg, *Rev. Anal. Chem.*, 2017, submitted.

3 N. Heidenreich, U. Rütt, M. Köppen, A. K. Inge, A.-C. Dippel, R. Suren and N. Stock, manuscript in preparation.

4 E. Antonova, B. Seidlhofer, J. Wang, M. Hinz and W. Bensch, *Chem. – Eur. J.*, 2012, **18**, 15316–15322.

5 L. Engelke, M. Schaefer, M. Schur and W. Bensch, *Chem. Mater.*, 2001, **13**, 1383.

6 R. Kiebach, N. Pienack, M.-E. Ordolff, F. Studt and W. Bensch, *Chem. Mater.*, 2006, **18**, 1196.

7 R. Kiebach, M. Schaefer, F. Porsch and W. Bensch, *Z. Anorg. Allg. Chem.*, 2005, **631**, 369.

8 N. Pienack, C. Näther and W. Bensch, *Eur. J. Inorg. Chem.*, 2009, **7**, 937.

9 T. Ahnfeldt, J. Moellmer, V. Guillerm, R. Staudt, C. Serre and N. Stock, *Chem. – Eur. J.*, 2011, **17**, 6462–6468.

10 R. El Osta, M. Feyand, N. Stock, F. Millange and R. I. Walton, *Powder Diffr.*, 2013, **28**, S256.

11 S. V. Dorozhkin, *Materials*, 2009, **2**, 399 and references therein.

12 H. Pan, S. Jiang, T. Zhang and R. Tang, *Methods Enzymol.*, 2013, **532**, 129.

13 R. Z. LeGeros, *J. Dent. Res.*, 1974, **53**, 45.

14 S. Takagi, L. C. Chow and K. Ishikawa, *Biomaterials*, 1998, **19**, 1593.

15 G. Willmann, *Adv. Eng. Mater.*, 1999, **1**, 95.

16 A. S. Posner and F. Betts, *Acc. Chem. Res.*, 1975, **8**, 273.

17 D. Gebauer, M. Kellermeier, J. D. Gale, L. Bergström and H. Cölfen, *Chem. Soc. Rev.*, 2014, **43**, 2348.

18 S. Bach, V. R. Celinski, M. Dietzsch, M. Panthöfer, R. Bienert, F. Emmerling, J. Schmedt auf der Günne and W. Tremel, *J. Am. Chem. Soc.*, 2015, **137**, 2285.

19 X. Yang, B. Xie, L. Wang, Y. Qin, Z. J. Henneman and G. H. Nancollas, *CrystEngComm*, 2011, **13**, 1153.

20 C.-G. Wang, J.-W. Liao, B.-D. Gou, J. Huang, R.-K. Tang, J.-H. Tao, T.-L. Zhang and K. Wang, *Cryst. Growth Des.*, 2009, **9**, 2620.

21 G. B. Ramirez-Rodriguez, J. M. Delgado-Lopez and J. Gomez-Morales, *CrystEngComm*, 2013, **15**, 2206.

22 E. I. Dorozhkina and S. V. Dorozhkin, *Colloids Surf., A*, 2002, **203**, 237.

23 R. Tang, Z. J. Henneman and G. H. Nancollas, *J. Cryst. Growth*, 2003, **249**, 614.

24 J. V. Rau, M. Fosca and V. S. Komlev, *Key Eng. Mater.*, 2013, **541**, 115.

25 Q. Zhang, Y. Jiang, B.-D. Gou, J. Huang, Y.-X. Gao, J.-T. Zhao, L. Zheng, Y.-D. Zhao, T.-L. Zhang and K. Wang, *Cryst. Growth Des.*, 2015, **15**, 2204.

26 H. Terraschke, L. R. Arana, P. Lindenberg and W. Bensch, *Analyst*, 2016, **141**, 2588.

27 H. Terraschke and C. Wickleder, *Chem. Rev.*, 2015, **115**, 11352.

28 H. Terraschke, M. Suta, M. Adlung, S. Mammadova, N. Musayeva, R. Jabbarov, M. Nazarov and C. Wickleder, *J. Spectrosc.*, 2015, **2015**, 541958.

29 H. Terraschke, M. F. T. Meier, Y. Voss, H. Schönherr and C. Wickleder, *J. Cer. Proc. Res.*, 2015, **16**, 59.

30 P. Dorenbos, *J. Lumin.*, 2013, **135**, 93.

31 K. Binnemans, *Coord. Chem. Rev.*, 2015, **295**, 1.

32 C. Gorller-Walrand and K. Binnemans, *Handb. Phys. Chem. Rare Earths*, 1996, **23**, 121.

33 G. Jia, P. A. Tanner, C.-K. Duan and J. Dexpert-Ghys, *J. Phys. Chem. C*, 2010, **114**, 2769.

1164 | *Inorg. Chem. Front.*, 2017, **4**, 1157–1165

This journal is © the Partner Organisations 2017

34 G. Blasse and B. C. Grabmaier, in *Luminescent Materials*, Springer, Berlin, 1994.

35 G. Li, Y. Tian, Y. Zhao and J. Lin, *Chem. Soc. Rev.*, 2015, **44**, 8688.

36 R. D. Shannon and C. T. Prewitt, *Acta Crystallogr., Sect. B: Struct. Crystallogr. Cryst. Chem.*, 1969, **25**, 925.

37 A. Dey, P. H. H. Bomans, F. A. Müller, J. Will, P. M. Frederik, G. de With and N. A. J. M. Sommerdijk, *Nat. Mater.*, 2010, **9**, 1010.

38 I. V. Berezovskaya, N. P. Efryushina, E. V. Zubar and V. P. Dotsenko, *Distribution and Luminescent Properties of Ce³⁺ Ions in Nanosized Calcium Hydroxyapatite*, Sumy State University, 2012, vol. 1, p. 01PCN24.

39 W. M. Yen, H. Yamamoto and S. Shionoya, in *Phosphor Handbook*, CRC Press Laser and Optical Science and Technology, Boca Raton, 2006.

40 T. Moon, S.-T. Hwang, D.-R. Jung, D. Son, C. Kim, J. Kim, M. Kang and B. Park, *J. Phys. Chem. C*, 2007, **111**, 4164.

41 C. A. Beevers, *Acta Crystallogr.*, 1958, **11**, 273.

42 M. I. Kay, R. A. Young and A. S. Posner, *Nature*, 1964, **204**, 1050.

43 L.-W. Du, S. Bian, B.-D. Gou, Y. Jiang, J. Huang, Y.-X. Gao, Y.-D. Zhao, W. Wen, T.-L. Zhang and K. Wang, *Cryst. Growth Des.*, 2013, **13**, 3103.

44 S. V. Dorozhkin, *Adv. Mater. Sci. Res.*, 2013, **15**, 1.

45 N. Pienack, L. Ruiz Arana, W. Bensch and H. Terraschke, *Crystals*, 2016, **6**, 157/1.

46 W. E. Brown, *Nature*, 1962, **196**, 1048.

47 A. Beeby, I. M. Clarkson, R. S. Dickins, S. Faulkner, D. Parker, L. Royle, A. S. de Sousa, J. A. Gareth Williams and M. Woods, *J. Chem. Soc., Perkin Trans. 2*, 1999, 493.

48 F. Chen, Y.-J. Zhu, K.-H. Zhang, J. Wu, K.-W. Wang, Q.-L. Tang and X.-M. Mo, *Nanoscale Res. Lett.*, 2011, **6**, 67.

49 R. Ternane, M. Trabelsi-Ayedi, N. Kbir-Ariguib and B. Piriou, *J. Lumin.*, 1999, **81**, 165.

50 O. A. Graeve, R. Kanakala, A. Madadi, B. C. Williams and K. C. Glass, *Biomaterials*, 2010, **31**, 4259.

51 C. S. Ciobanu, S. L. Iconaru, F. Massuyeau, L. V. Constantin, A. Costescu and D. Predoi, *J. Nanomater.*, 2012, 942801.

52 C. Sun and D. Xue, *J. Phys. Chem. C*, 2013, **117**, 19146.

53 A.-C. Dippel, H.-P. Liermann, J. T. Delitz, P. Walter, H. Schulte-Schrepping, O. Seeck and H. Franz, *J. Synchrotron Radiat.*, 2015, **22**, 675.

54 O. H. Seeck, C. Deiter, K. Pflaum, F. Bertam, A. Beerlink, H. Franz, J. Horbach, H. Schulte-Schrepping, B. M. Murphy, M. Greve and O. Magnussen, *J. Synchrotron Radiat.*, 2012, **19**, 30.

55 M. Wendt, L. K. Mahnke, N. Heidenreich and W. Bensch, *Eur. J. Inorg. Chem.*, 2016, 5393.

56 L. Engelke, M. Schaefer, F. Porsch and W. Bensch, *Eur. J. Inorg. Chem.*, 2003, **3**, 506–513.

This journal is © the Partner Organisations 2017

Inorg. Chem. Front., 2017, **4**, 1157–1165 | **1165**